Bioorganic Chemistry 85 (2019) 445–454

Contents lists available at ScienceDirect

Bioorganic Chemistry

journal homepage: www.elsevier.com/locate/bioorg

Novel hybrids of podophyllotoxin and formononetin inhibit the growth, migration and invasion of lung cancer cells

Chengli Yang, Qiongli Xie, Xian Zeng, Nengyin Tao, Yingshu Xu, Yongzheng Chen, Jing Wang*, Lei Zhang*

Generic Drug Research Center of Guizhou Province, Green Pharmaceuticals Engineering Research Center of Guizhou Province, School of Pharmacy, Zunyi Medical University, Zunyi 563003, PR China

ARTICLE INFO

Keywords:
Podophyllotoxin
Formononetin
Hybridization
Antiproliferative activity
Migration
Invasion

ABSTRACT

In this study, three hybrids of podophyllotoxin and formononetin were synthesized and evaluated for anticancer efficacy. Some of the derivatives exhibited potent cytotoxicity against a panel of human and mouse cancer cell lines, with IC_{50} values in the low micromolar to submicromolar range. Evaluation against A549 lung tumor cell line identified that the IC_{50} value of compound **10a** was 0.753 μM, indicating that **10a** was 2.568-fold more efficacious than parent podophyllotoxin. Mechanistic studies revealed that **10a** induced A549 cell apoptosis mainly via caspase pathway, as well as disrupted the microtubule organization by occupying the colchicine binding site of the tubulin. Moreover, wound healing assay and transwell invasion assay indicated that **10a** displayed potent inhibitory effects on invasion and migration in A549 cancer cells. In additiona, a decrease in vimentin immunostaining was also observed in A549 cells after treatment with **10a**. Overall, hybrid **10a** might be a promising candidate for the potential treatment of human lung carcinoma.

1. Introduction

Cancer has been regarded as a leading cause of death in China, according to the National Central Cancer Registry of China [1]. Although considerable progresses in cancer therapy have been reported, the development of novel anticancer drugs is still a challenge in medicinal chemistry.

Natural products are considered as “privileged structures” due to their diverse curative potential [2]. Among them, cyclolignans represent a unique chemical class, such as podophyllotoxin (**1**, Fig. 1). Podophyllotoxin, derived from *Podophyllum species*, has attracted much attention for its various biological activities, such as antirheumatic, antiviral and pesticidal properties [3]. More importantly, podophyllotoxin shows interesting antiproliferative effect against many different types of cancers, such as breast cancer, prostate cancer, colon cancer and osteosarcoma, by the inhibition of tubulin polymerization [4]. However, serious side effects like nausea, diarrhea, vomiting have hindered its use as an efficient anticancer agent. To overcome these drawbacks, various structure modification of podophyllotoxin have been performed worldwide [5]. In particularly, the two semisynthetic glucosidic derivatives, etoposide (**2**, Fig. 1) and teniposide (**3**, Fig. 1), are widely used as anticancer drugs in the chemotherapy of lung cancer, lymphomas and Kaposi's sarcoma [6]. Intriguingly, these two drugs are topoisomerase II inhibitors [7]. However, the two clinic drugs have been reported to own some issues, such as poor bioavailability and drug resistance. Due to the toxic effects of podophyllotoxin and its derivatives, there is an urgent need for the development of more potent and/or less toxic analogs of this natural product. Structure-activity relationship and molecular docking experiments have unambiguously indicated that C4 of podophyllotoxin is the major site tolerant to structural diversification [8,9]. At present, extensive efforts have been made [10]. For example, a series of *N*-(aminosulfonyl)-4-podophyllotoxin carbamates were synthesized by Xu and coworkers. Among them, *N*-(morpholinosulfonyl)-4-podophyllotoxin carbamate **4** (Fig. 1) exhibited potent anticancer activity against HeLa cells (IC_{50} = 0.5 μM). In addition, compound **4** could induce cell cycle arrest in the G2/M phase, and inhibit tubulin polymerization and microtubule assembly in HeLa cells [11]. Piperazine acetate podophyllotoxin ester derivative **5** (Fig. 1) was proved to manifest selectively prominent cytotoxicity towards MCF-7 cells in MTT assay, with an IC_{50} value of 2.78 μM, and displayed low cytotoxicity against human normal L02 cells. Moreover, compound **5** could block cell cycle at G2 phase, and inhibit the microtubule network in MCF-7 cells as well [12]. More recently, our group reported that the podophyllotoxin-pterostilbene fused conjugate **6** (Fig. 1)

* Corresponding authors.
E-mail addresses: wangjing@zmc.edu.cn (J. Wang), lzhang@zmc.edu.cn (L. Zhang).

https://doi.org/10.1016/j.bioorg.2019.02.019
Received 30 September 2018; Received in revised form 22 January 2019; Accepted 6 February 2019
Available online 06 February 2019
0045-2068/

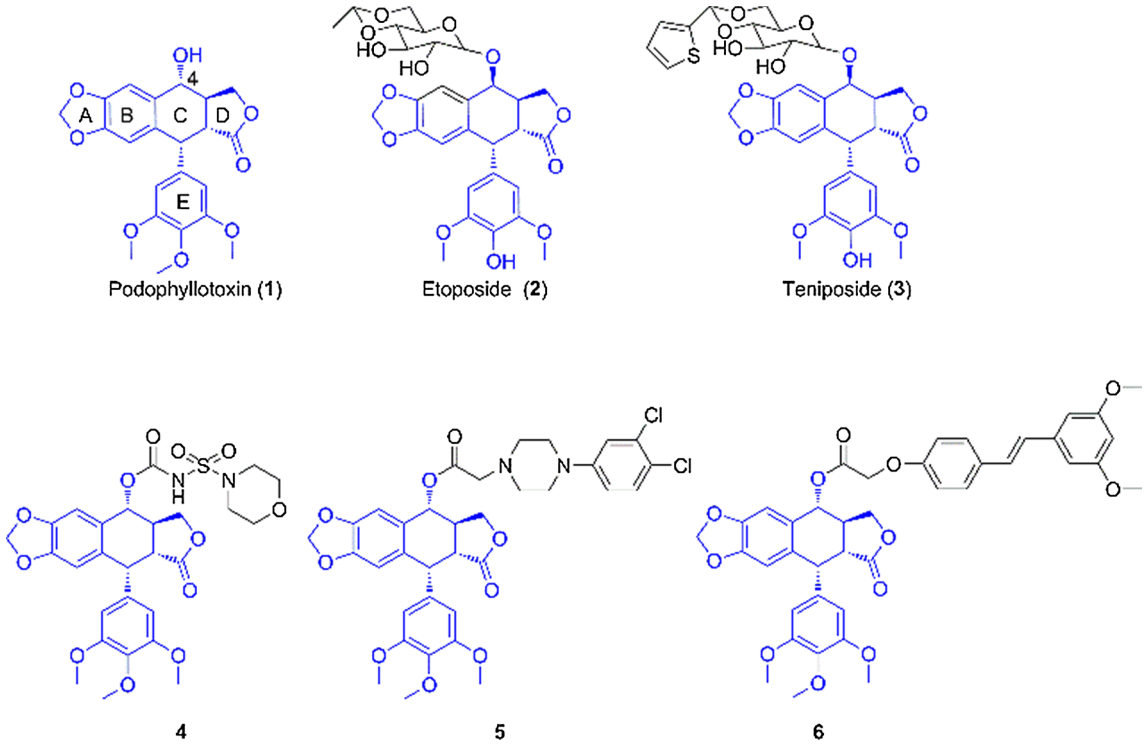

Fig. 1. The structures of podophyllotoxin and its analogues.

exhibited a significant IC_{50} value of 0.081 μM against MUM-2B melanoma cells. Importantly, compound **6** showed antimigratory activity via up-regulating the level of E-cadherin, and down-regulating the expression of VEGFR-2 and MMP-2 in MUM-2B cells [13].

Formononetin (**7**, Fig. 2) is an isoflavone found in *Leguminosae* family, such as *Trifolium pretense* and *Glycyrrhiza*. It has previously been reported to have many potent biological activities, including antidiabetic, antioxidant, antiangiogenic, antimycobacterial, neuroprotective, anti-inflammatory effects, and so on [14–17]. Recently, formononetin has attracted broad attention for its potential anticancer activity against many cancer cell lines, such as A549, HCT116, A2780 and MDA-MB-231 and U266 cells [18–22], and many formononetin derivatives were prepared as antiproliferative agents and explored their pharmacological mechanism [23,24]. For example, Ren et al. reported that formononetin nitrogen mustard derivatives **8** (Fig. 2) showed potent antitumor activity against HCT-116 cells with an IC_{50} value of 3.8 μM, and induced cell cycle arrest at G2/M phase and cell apoptosis [25]. In addition, formononetin-dithiocarbamate hybrid **9** (Fig. 2) was proved to arrest cell cycle, and inhibit cell growth and migration via MAPK/Wnt signaling pathways in PC-3 cells, with an IC_{50} value of 1.97 μM [26].

Molecular hybridization is an attractive structural modification strategy to design of new molecules based on the combination of two or more bioactive compounds or pharmacophoric units [27]. Additionally, a number of lines of evidence have demonstrated that C4 of podophyllotoxin was tolerant of structural diversification, and the C4 substituent was reported to insert into a hydrophobic cavity of a-tubulin or the narrow gap in αβ-interface, which might provid more enhanced anticancer activity [28–31]. These above interesting findings and our ongoing efforts to develop potent anticancer candidates, led to the molecular hybridization of podophyllotoxin and formononetin to integrate them in one molecule to create new hybrid (**10**, Fig. 3) with excellent antiproliferative activity. To verify the hypothesis, herein, we reported the synthesis of novel hybrids of podophyllotoxin and formononetin using a molecular hybridization approach, as well as the evaluation of their antitumor efficacy *in vitro*. In addition, the underlying mechanism of the representative hybrid was also evaluated in the current study.

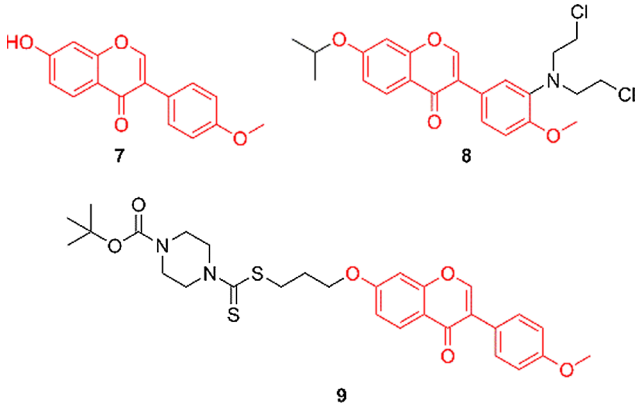

Fig. 2. The structures of formononetin and its analogues.

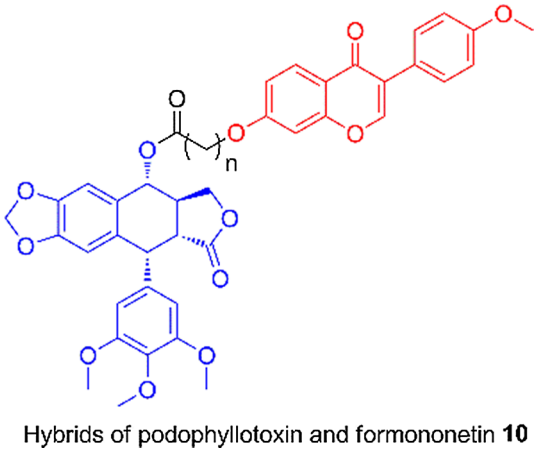

Fig. 3. Targeted hybrids of podophyllotoxin and formononetin.

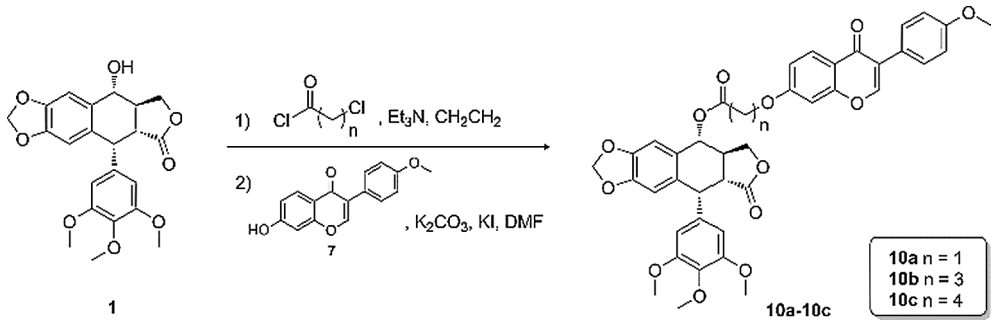

Scheme 1. Synthesis of hybrids of podophyllotoxin and formononetin.

Table 1
In vitro antiproliferative activities of compounds.

Compound	IC_{50} (μM)[a]							
	SKOV3	MCF-7	HepG2	HeLa	A549	CT26	B16f10	HUVEC
10a	0.213 ± 0.112	2.384 ± 0.408	0.277 ± 0.031	0.763 ± 0.244	0.753 ± 0.173	0.679 ± 0.109	1.066 ± 0.366	0.568 ± 0.130
10b	2.128 ± 0.841	20.775 ± 7.688	2.447 ± 0.866	3.559 ± 0.338	7.656 ± 1.907	3.240 ± 0.338	1.715 ± 0.763	20.409 ± 6.234
10c	2.182 ± 1.626	74.556 ± 11.198	1.524 ± 0.290	2.752 ± 1.039	4.116 ± 1.445	5.739 ± 1.070	2.431 ± 0.546	28.356 ± 9.347
1	0.096 ± 0.075	1.059 ± 0.549	0.153 ± 0.025	0.375 ± 0.155	1.934 ± 0.089	0.411 ± 0.290	0.611 ± 0.118	0.236 ± 0.098
7	> 50	> 50	> 50	> 50	> 50	> 50	> 50	46.389 ± 14.346

[a] Cell lines were incubated with compounds for 72 h. Cell viability was measured by MTT assay as described in the Experimental Section. IC_{50} values were indicated as mean IC_{50} ± SD (μM).

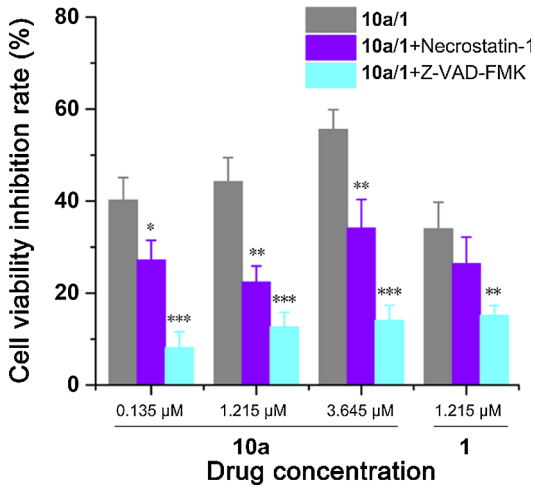

Fig. 4. Cytotoxicity effects. A549 cells were treated with **10a** and **1** for 48 h in the absence or presence of Necrostatin-1 (10 μM) or Z-VAD-FMK (20 μM). The control cells were treated with DMSO. The cell viability was measured by MTT assay. Necrostatin-1 or Z-VAD-FMK was pretreated for 1 h. The cytotoxicity was descripted as: cell viability inhibition rate (%) = (MTT value of control group - MTT value of treated group)/MTT value of control group. * represents $p < 0.05$, ** represents $p < 0.01$ and *** represents $p < 0.001$.

2. Results and discussion

2.1. Chemistry

The general synthetic route for the hybrids of podophyllotoxin and formononetin was illustrated in Scheme 1. Initially, podophyllotoxin was reacted with chloro acyl chloride in triethylamine and dichloromethane by esterification. The hybrids **10a-10c** were obtained via nucleophilic substitution reaction of above intermediate and formononetin in the presence of potassium iodide and potassium carbonate. All compounds were fully characterized by ^{1}H NMR, ^{13}C NMR and high-resolution mass spectrometry.

2.2. Biology

2.2.1. MTT assay

To evaluate the antiproliferative effects of the hybrids of podophyllotoxin and formononetin, compounds **10a-10c** were screened for cytotoxic activity against a panel of seven different cancer cell lines [SKOV3 (human ovarian carcinoma), MCF-7 (human breast carcinoma), HepG2 (human hepatocellular carcinoma), HeLa (human cervical carcinoma), A549 (human lung carcinoma), CT26 (mouse colon carcinoma), B16f10 (mouse melanoma carcinoma)] and a human endothelial cell line [HUVEC (human umbilical vein endothelial cell)]. Podophyllotoxin (**1**) and formononetin (**7**) were used as positive compounds. As shown in Table 1, three hybrids not only displayed significantly antiproliferative activity against human cancer cell lines with IC_{50} values varying from low micromolar to submicromolar range, but also exhibited growth inhibitory effects on mouse cancer cell lines. Among them, hybrids displayed more potent activity against SKOV3 and HepG2 cells. Moreover, the results showed that compound **10a**, possessing two carbon chain, exhibited more potent activity than the other two compounds with longer chains, **10b** and **10c**, against all cancer cell lines. For example, the IC_{50} values of **10a** against SKOV3 and HepG2 cells were 0.213 and 0.277 μM, respectively. However, no significant antiproliferative activity was observed in cells exposed to positive compound formononetin. And as expected, natural product podophyllotoxin exhibited excellent antiproliferative activity. Interestingly, among the test cancer lines, only one, A549 cell line, was observed more sensitive to hybrid (**10a**) than parent podophyllotoxin, meaning the IC_{50} value of **10a** was 2.568-fold more potent than podophyllotoxin. Additionally, angiogenesis is an essential process during tumorigenesis, and podophyllotoxin was reported to inhibit this process. For example, Guo et al. showed that podophyllotoxin had an obvious effect on antiangiogenisis of chick chorioallantoic membrane [32]. As shown in Table 1, compound **10a** was more active towards HUVEC cells among the hybrids of podophyllotoxin and formononetin, indicating that **10a** might reveal antiangiogenic activity and have potential ability to inhibit tumor growth, but the effect was slightly weaker than parent **1**.

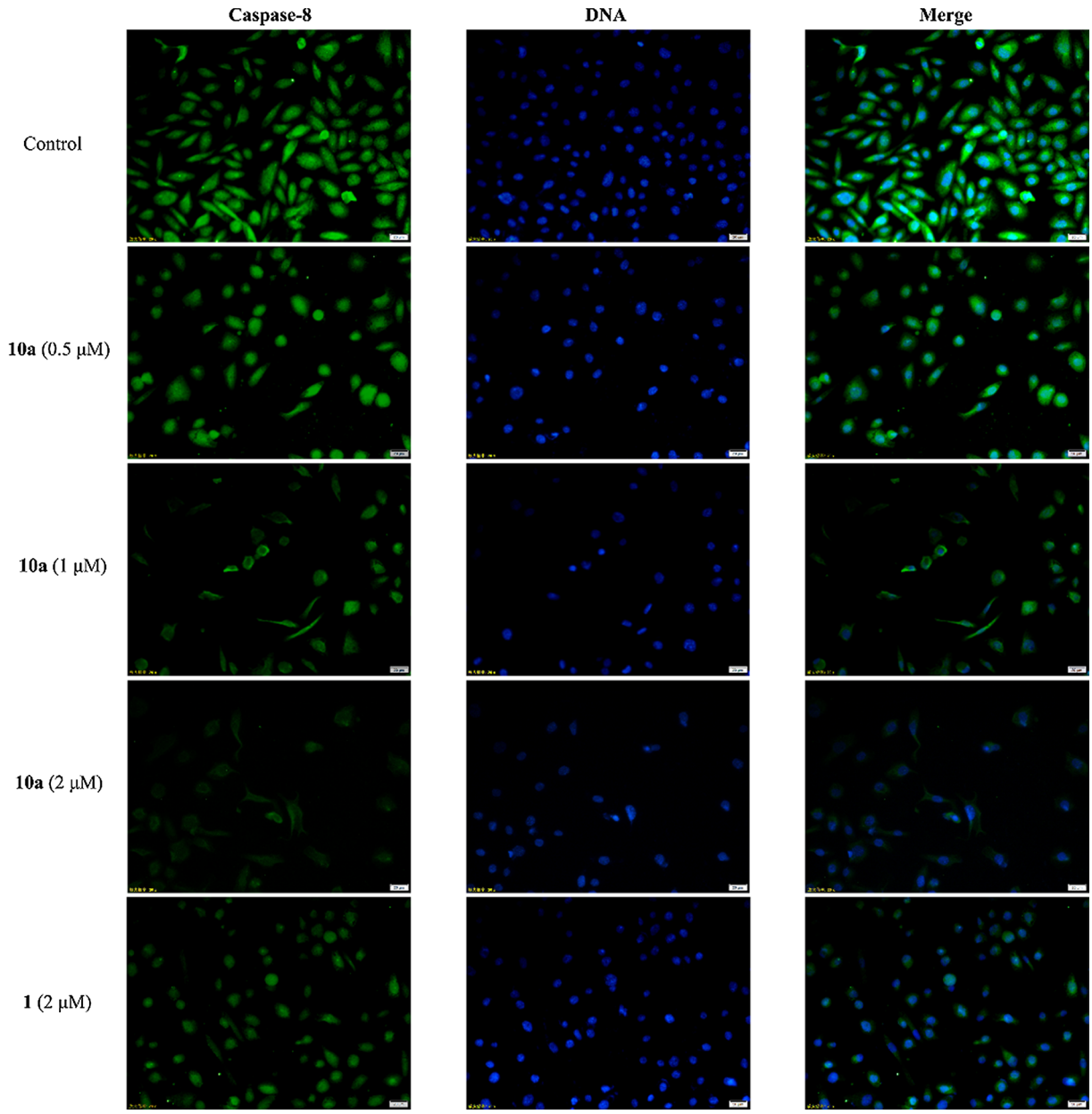

Fig. 5. The distribution of caspase-8 in A549 cells. A549 cells were incubated with vehicle, **10a** and **1** for 24 h, respectively. Nucleuses were stained with DAPI (blue), and caspase-8 were stained with anti-caspase-8 antibody (green). Magnification 20×.

2.2.2. MTT using Necrostatin-1 & Z-VAD-FMK

To investigate the mechanism of how hybrid **10a** killed lung carcinoma, we further added necroptosis inhibitor or apoptosis inhibitor prior to drug treatment. A549 cell viability was measured for 48 h by MTT assay. The cytotoxicity was descripted as cell viability inhibition rate (%). Firstly, after treatment with **10a** at the concentrations of 0.135, 1.215 and 3.645 μM, the cell viability inhibition rate (%) was increased to 40.160, 44.257 and 55.622 (Fig. 4), respectively, indicating that **10a** inhibited A549 cell viability in a dose-dependent manner. However, above inhibition was attenuated by pretreatment with 10 μM Necrostatin-1 (a potent necroptosis inhibitor) or 20 μM Z-VAD-FMK (a general caspase inhibitor). Similar tendency was observed in **1**-treated group. The results indicated that hybrid **10a** might induce cell death in A549 cells mainly via caspase pathway.

2.2.3. Immunofluorescence of Caspase-8

Caspases play a crucial role in the apoptotic process [33]. And caspase-8 acts as the most upstream caspase in apoptotic signaling. To investigate this further, we used an immunofluorescence approach to determine the distribution of caspase-8 in **10a**-treated A549 cells. As shown in Fig. 5, in untreated A549 cells, caspase-8 was preferentially detected as green fluorescence in the perinuclear cytoplasm. After the treatment of A549 cells with **10a** at the concentrations of 0.5, 1 and 2 μM for 24 h, the decreased green fluorescence of caspase-8 was observed in a concentration-dependent manner, which suggested that the **10a** could suppress the expression of caspase-8 in A549 cells. Similar phenomenon was observed in **1**-treated group.

2.2.4. Acridine orange/ethidium bromide (AO/EB) dual staining

To evaluate the effect of **10a** on apoptosis in A549 cells, acridine orange (AO) and ethidium bromide (EB) were used as fluorescent probes. The morphological analysis was depicted in Fig. 6. In the control group, A549 cells were stained with uniform green fluorescence and cell nucleus presented intact. After treatment with **10a** for a period of 24 h, it was found that the cells which were dyed to light orange fluorescence exhibited the representative apoptotic features, such as

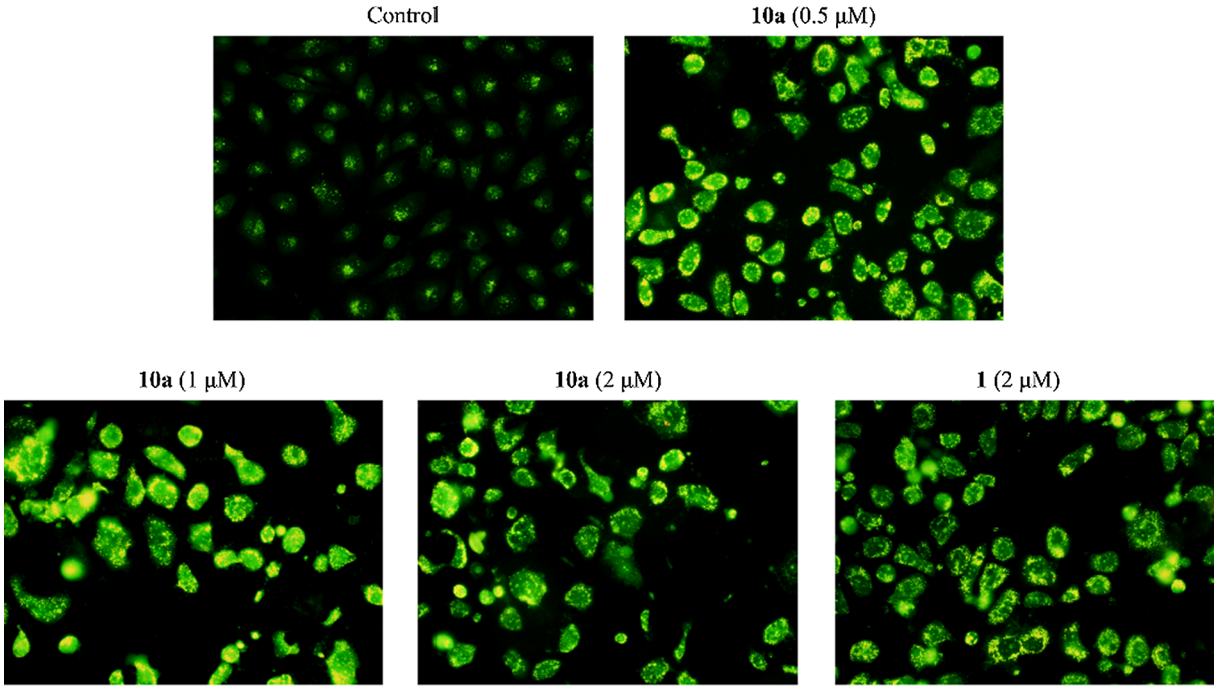

Fig. 6. A549 cells were stained by AO/EB and detected under fluorescence microscopy. A549 cells were incubated with vehicle, **10a** and **1** for 24 h, respectively. The cells were stained with AO/EB. Magnification 20 × .

cell shrinkage and chromatin condensation. Similar result was also observed in the cells incubated with compound **1**. The results indicated that hybrid **10a** could induce apoptosis in A549 lung cancer cells.

2.2.5. Immunofluorescence of microtubules

To investigate whether the hybrid **10a** was a tubulin-targeting agent, we further examined the effect of **10a** on the cellular microtubule network by using immunofluorescence staining. As shown in Fig. 7, the untreated A549 cells exhibited a normal arrangement and organization of microtubule. By contrast, after 24 h of exposure to **10a**, the microtubule polymerization and spindle formation became disorganized. Similar phenomenon was also observed in **1**-treated group. These data revealed that compound **10a** induced depolymerization of microtubule network in A549 cells.

2.2.6. Molecular modeling

To further elucidate the binding mechanism of the hybrid **10a**, molecular modeling of **10a** was performed into the tubulin (PDB code: 1SA0) by using the GLIDE module in Schrödinger suite. As shown in Fig. 8, the trimethoxyphenyl ring in **10a** occupied the colchicine binding site of β-subunit as expected. The formononetin ring was located close to the αβ-interface, and formed a hydrogen bond with LEU-248 residue (d = 3.1 Å) from the β-subunit. The docking results showed that hybrid **10a** disrupted the microtubule network by occupying the colchicine binding site of the tubulin.

2.2.7. Wound healing assay

The progression and metastasis of cancer are dependent on invasion and migration of malignant cells [34]. In the present study, wound healing assay was performed to investigate the effect of hybrid **10a** on the migration of A549 cells. A549 is a type of human non-small cell lung cancer (NSCLC) that is prone to migration and invasion [35]. After the compounds treatment of 0 h and 24 h, we captured the images of the injured area. The inhibition of the cell migration rate was quantified and compared with that of untreated cells. As shown in Fig. 9, the wound area was almost completely healed in DMSO-treated control after 24 h. In contrast, compound **10a** inhibited the A549 migration in a dose-dependent manner. What's more, similar inhibition of cell migration was observed in **1**-treated group. These results demonstrated that **10a** had the ability to inhibit the migration capability of A549 cells.

2.2.8. Transwell invasion assay

In order to further determine the anti-invasion effect of compound **10a**, *in vitro* transwell assay was performed on A549 cells. The inhibition of the cell invasion rate was quantified and compared with that of untreated cells. The results in Fig. 10 revealed that compound **10a** markedly decreased A549 tumor cell invasion at various concentrations (0.05 and 0.5 μM). In addition, the inhibitory effect on invasion of **10a** at 0.5 μM was similar to that of compound **1** at 0.5 μM. The results indicated that **10a** significantly inhibited A549 cell invasion in a concentration-dependent manner.

2.2.9. Immunofluorescence of vimentin

Vimentin, an intermediate filament protein, is associated with increased metastasis and poor prognosis for non-small cell lung cancer patients [36]. Mounting evidence implicates vimentin as a key regulator of lung adenocarcinoma invasion and metastasis [37,38]. Thus, we evaluated the effect of compound **10a** on the vimentin filament distribution by mean of immunofluorescence staining assays in A549 lung cancer cells. As shown in Fig. 11, A549 cells in control group exhibited a normal organization of vimentin filaments. However, treatment with compound **10a** induced a morphological rearrangement of vimentin filaments dose-dependently. Similar phenomenon was found in **1**-treated group. These results indicated that compound **10a** might inhibit invasion and migration of A549 cells via degradation of vimentin filaments.

3. Conclusion

Podophyllotoxin, a tubulin polymerization inhibitor, was reported to bind at the colchicine site of tubulin. Meanwhile, high resolution crystal structure showed that 3,4,5-trimethoxybenzoyl at ring-E of podophyllotoxin was located deeply inside the colchicine binding site [39], and substituent at the C4 hydroxyl could insert into a

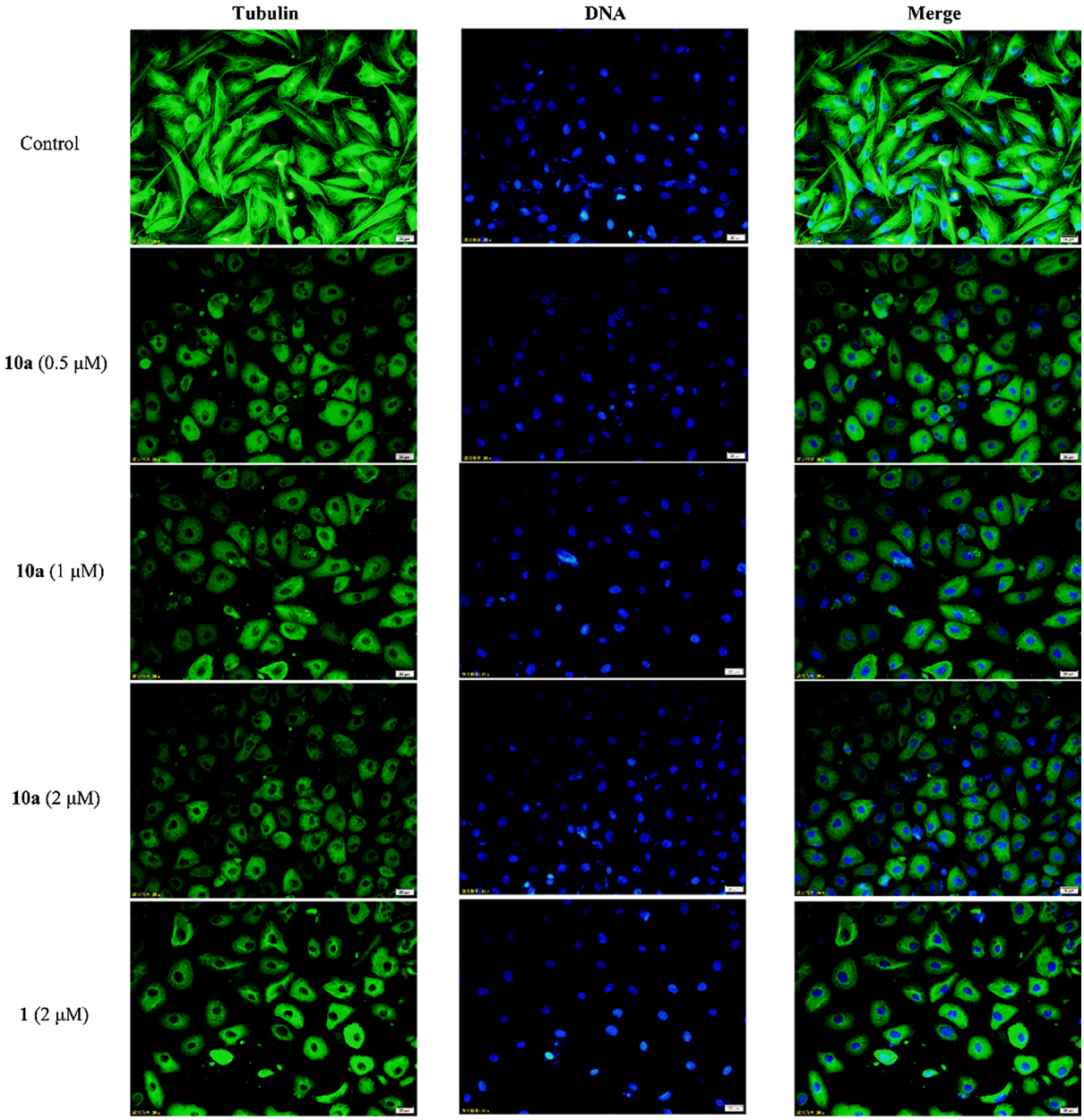

Fig. 7. Effects of **10a** on the microtubule network in A549 cells. A549 cells were incubated with vehicle, **10a** and **1** for 24 h, respectively. Microtubules were visualized with anti-α-tubulin antibody (green), and cell nuclei were stained with DAPI (blue). Magnification 20×.

hydrophobic cavity of a-tubulin or the narrow gap in αβ-interface, probably resulting in an enhanced anticancer activity [12]. In present study, three hybrids of podophyllotoxin bearing natural product formononetin fragment at C4 hydroxyl position were synthesized. Among them, molecule **10a** with shortest linker showed the best antineoplastic activity, and its A549 tumor growth inhibition activity was stronger than that of podophyllotoxin (Table 1). Moreover, the formononetin fragment in **10a** could insert into the αβ-interface, and formed a hydrogen bond (Fig. 8), leading to the destruction of tubulin cytoskeleton (Fig. 7).

Migration and invasion have been reported to play important roles in the progression and metastasis of neoplasm [40]. The results of wound healing assay, transwell invasion assay and immunofluorescence of vimentin demonstrated that compound **10a** could significantly inhibit the migration (Fig. 9) and invasion (Fig. 10) of A549 lung cancer cells.

Our results demonstrated that hybrid **10a** might be a promising anticancer candidate. In the future, it will be interesting to evaluate its metabolic stability and *in vivo* efficiency.

4. Experimental

4.1. General

Melting points were determined on a SGWX-4 microscope meltingpoint apparatus and given uncorrected. ^{1}H and ^{13}C NMR analyses were performed using 400 MHz Agilent spectrometer. High resolution mass spectrometric data were determined on Agilent Accurate-Mass-Q-TOF-MS 6520. All analytical grade solvents and reagents were purchased from commercial sources and used without further purification.

4.2. General preparation of compounds *10a-10c*

A mixture of podophyllotoxin (0.1 mmol) and triethylamine

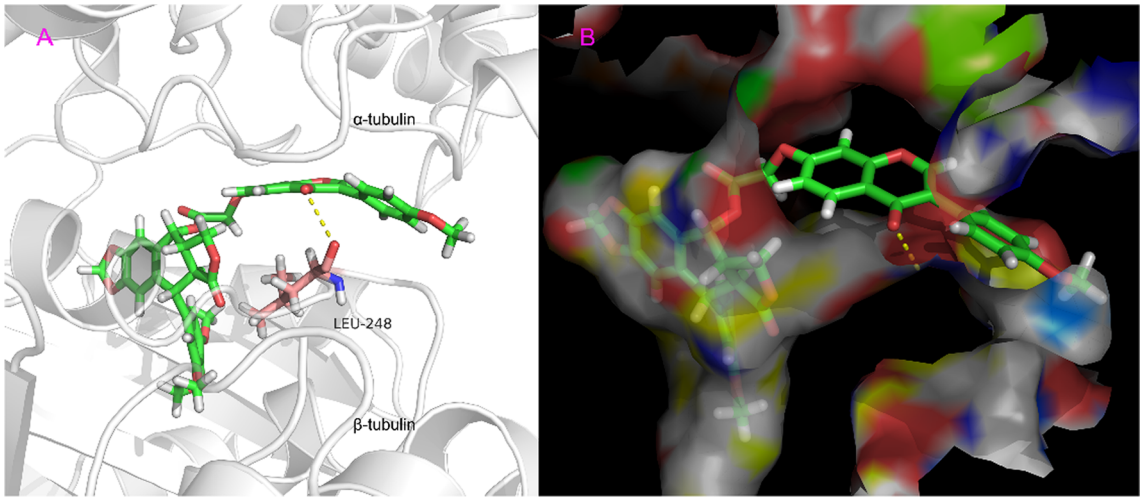

Fig. 8. The binding mode of compound **10a** (green color stick) in the colchicine site of tubulin. The docking pose was illustrated by two different visualizations: **A** (ribbon) and **B** (protein surface) representations. Yellow dashed line represented hydrogen bond.

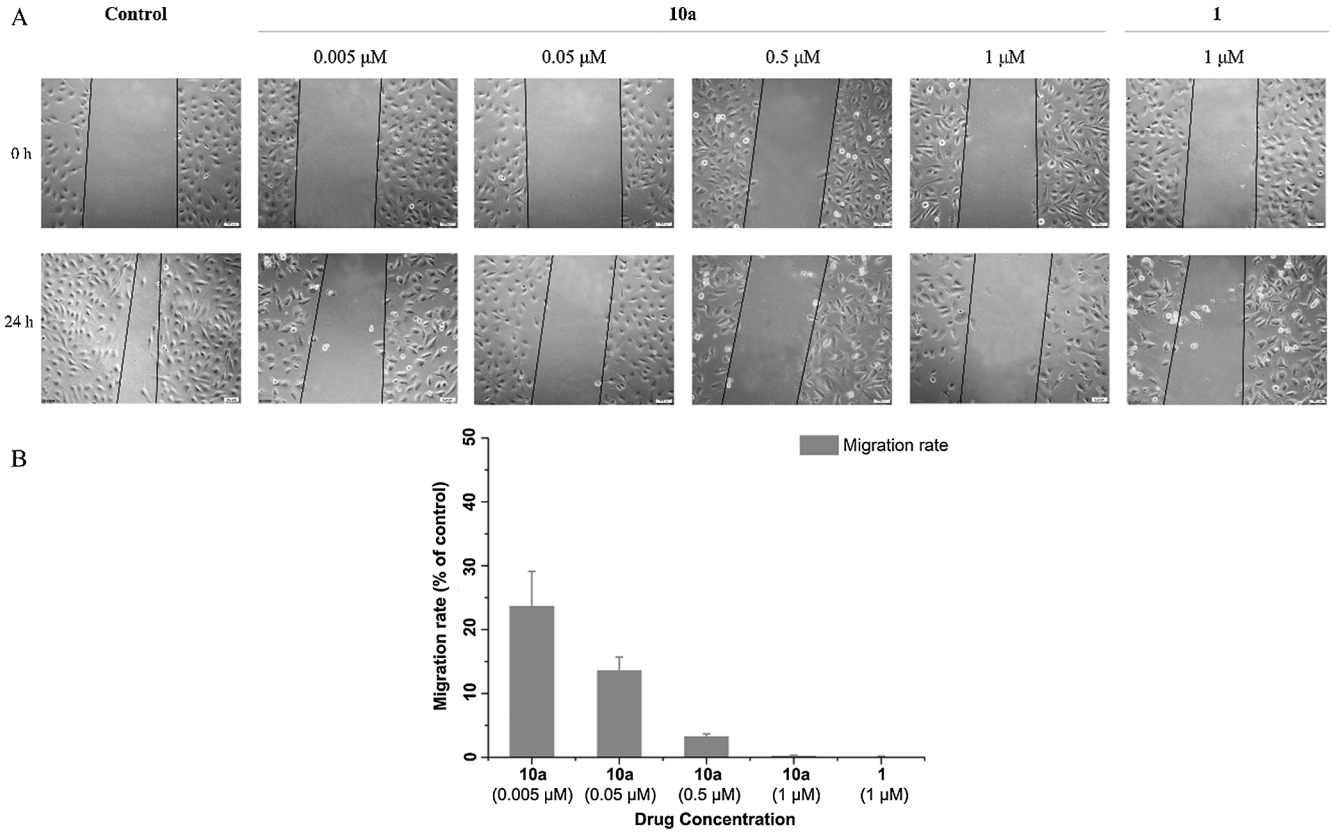

Fig. 9. Wound healing migration assay of A549 cells. (A) The images were captured before (0 h), and after 24 h of treatment with vehicle, **10a** and **1**. Magnification 20×. (B) Relative inhibition of cell migration in (A). The percentage of inhibition was calculated relative to untreated cells (control).

(0.5 mmol) in dichloromethane (5 mL) was stirred at 0 °C. Chloro acyl chloride (0.25 mmol) dissolved in dichloromethane (5 mL) was added slowly under stirring. The mixture was stirred at room temperature for 1 h, quenched with saturated NH_4Cl solution, and then extracted with dichloromethane for three times. And the organic layer was washed with brine, dried by Na_2SO_4, filtered, and removed by evaporation in vacuo. The crude product was used in the next reaction without further. A mixture of above residue product, formononetin (0.105 mmol), potassium carbonate (0.1 mmol) and catalytic amount KI was stirred in anhydrous DMF (3 mL) for 2 h at 100 °C under argon. Then, the mixture was quenched with brine and extracted with dichloromethane. The organic layer was washed with water and brine, dried with Na_2SO_4, filtered and removed by evaporation in vacuo. The residue was purified by silica gel chromatography to give pure compound.

*4.2.1. 4α-(4-((3-(4-methoxyphenyl)-4-oxo-4H-chromen-7-yl-acetyl)-4-desoxypodophyllotoxin (**10a**)*

White solid, yield 85%; mp: 133–35 °C; ^{1}H NMR (400 MHz, $CDCl_3$) δ 8.25 (d, J = 8.8 Hz, 1H), 7.92 (d, J = 5.2 Hz, 1H), 7.49 (d, J = 8.4 Hz, 2H), 7.01 (d, J = 9.2 Hz, 1H), 6.97 (d, J = 8.4 Hz, 2H), 6.85 (s, 1H), 6.56 (s, 1H), 6.52 (s, 1H), 6.35 (s, 2H), 6.01 (d, J = 8.8 Hz, 1H), 5.94 (s, 2H), 4.86 (d, J = 5.2 Hz, 1H), 4.59 (d, J = 3.2 Hz, 1H), 4.49–4.35 (m,

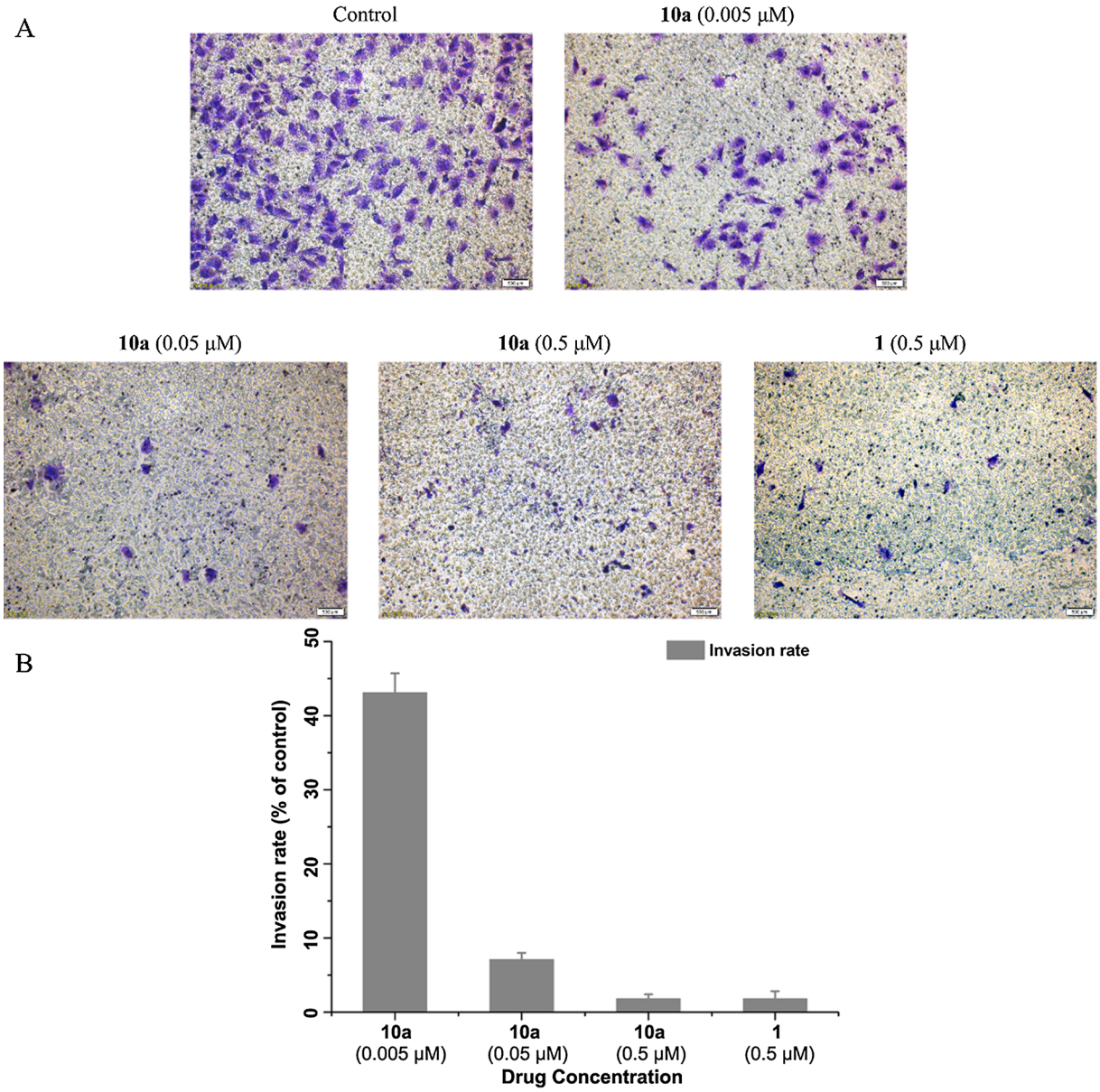

Fig. 10. The effects of **10a** on the invasion of A549 cells were assessed by transwell invasion assay. (A) Images of transwell invasion assay. A549 cells were treated with vehicle, **10a** and **1** at various concentrations. Magnification 20×. (B) Relative inhibition of cell invasion in (A). The percentage of inhibition was calculated relative to untreated cells (control).

2H), 4.20 (t, J = 9.6 Hz, 1H), 3.82 (s, 3H), 3.79 (s, 3H), 3.74 (s, 6H), 2.95–2.86 (m, 2H); ^{13}C NMR (100 MHz, $CDCl_3$) δ 176.78, 175.66, 173.27, 168.56, 161.49, 159.62, 157.57, 153.17, 152.64, 152.19, 148.37, 147.61, 137.15, 134.51, 132.52, 130.06, 128.45, 127.06, 125.05, 123.85, 119.44, 114.11, 113.98, 109.79, 107.99, 106.69, 105.37, 101.72, 101.28, 75.20, 71.03, 65.26, 60.76, 56.31, 56.14, 55.33, 45.50, 43.59, 38.47; HRMS-ESI (m/z): calcd for $C_{40}H_{35}O_{13}$ $[M+H]^+$ 723.2072, found 723.2063.

*4.2.2. 4α-(4-((3-(4-methoxyphenyl)-4-oxo-4H-chromen-7-yl-butyryl)-4-desoxypodophyllotoxin (**10b**)*

White solid, yield 71%; mp: 126–128 °C; ^{1}H NMR (400 MHz, $CDCl_3$) δ 8.18 (d, J = 8.8 Hz, 1H), 7.90 (s, 1H), 7.49 (d, J = 8.4 Hz, 2H), 6.96 (d, J = 8.4 Hz, 3H), 6.82 (d, J = 2.0 Hz, 1H), 6.73 (s, 1H), 6.37 (s, 2H), 5.96 (d, J = 10.0 Hz, 2H), 5.72 (d, J = 4.8 Hz, 1H), 4.43–4.37 (m, 2H), 4.31–4.25 (m, 1H), 4.02 (t, J = 6.0 Hz, 2H), 3.82 (s, 3H), 3.81 (s, 3H), 3.77 (s, 6H), 3.31–3.28 (m, 1H), 2.95 (s, 1H), 2.33–2.26 (m, 2H), 1.82–1.71 (m, 3H); ^{13}C NMR (100 MHz, $CDCl_3$) δ 177.22, 172.81, 163.13, 159.52, 157.86, 153.17, 152.03, 148.42, 147.22, 138.80, 131.21, 130.09, 127.74, 126.08, 124.14, 114.72, 113.92, 109.90, 108.37, 105.29, 101.44, 100.56, 72.49, 70.76, 67.89, 60.84, 56.14, 55.32, 45.38, 44.16, 39.68, 33.78, 28.35, 21.41; HRMS-ESI (m/z): calcd for $C_{42}H_{39}O_{13}$ $[M+H]^+$ 751.2385, found 751.2379.

*4.2.3. 4α-(4-((3-(4-methoxyphenyl)-4-oxo-4H-chromen-7-yl-valeryl)-4-desoxypodophyllotoxin (**10c**)*

White solid, yield 64%; mp: 111–113 °C; ^{1}H NMR (400 MHz, $CDCl_3$) δ 8.19 (d, J = 8.8 Hz, 1H), 7.90 (d, J = 4.4 Hz, 1H), 7.49 (d, J = 8.4 Hz, 2H), 6.96 (d, J = 8.4 Hz, 2H), 6.93 (d, J = 8.0 Hz, 1H), 6.81 (d, J = 2.8 Hz, 1H), 6.73 (d, J = 4.8 Hz, 1H), 6.55 (d, J = 4.0 Hz, 1H), 6.37 (s, 2H), 5.96–5.90 (m, 2H), 5.74–5.71 (m, 1H), 4.43 (d, J = 9.2 Hz, 1H), 4.39 (s, 1H), 4.31–4.25 (m, 1H), 4.07–4.00 (m, 2H), 3.82 (s, 3H), 3.81 (s, 3H), 3.77 (s, 6H), 3.30–3.27 (m, 1H), 2.97 (s, 1H), 2.46–2.39 (m, 1H), 2.31–2.24 (m, 1H), 2.11–2.04 (m, 1H), 1.85–1.69 (m, 3H); ^{13}C NMR (100 MHz, $CDCl_3$) δ 177.18, 172.52, 162.89, 159.54, 153.19, 152.04, 148.44, 147.22, 138.77, 131.22, 130.09, 127.85, 127.74,

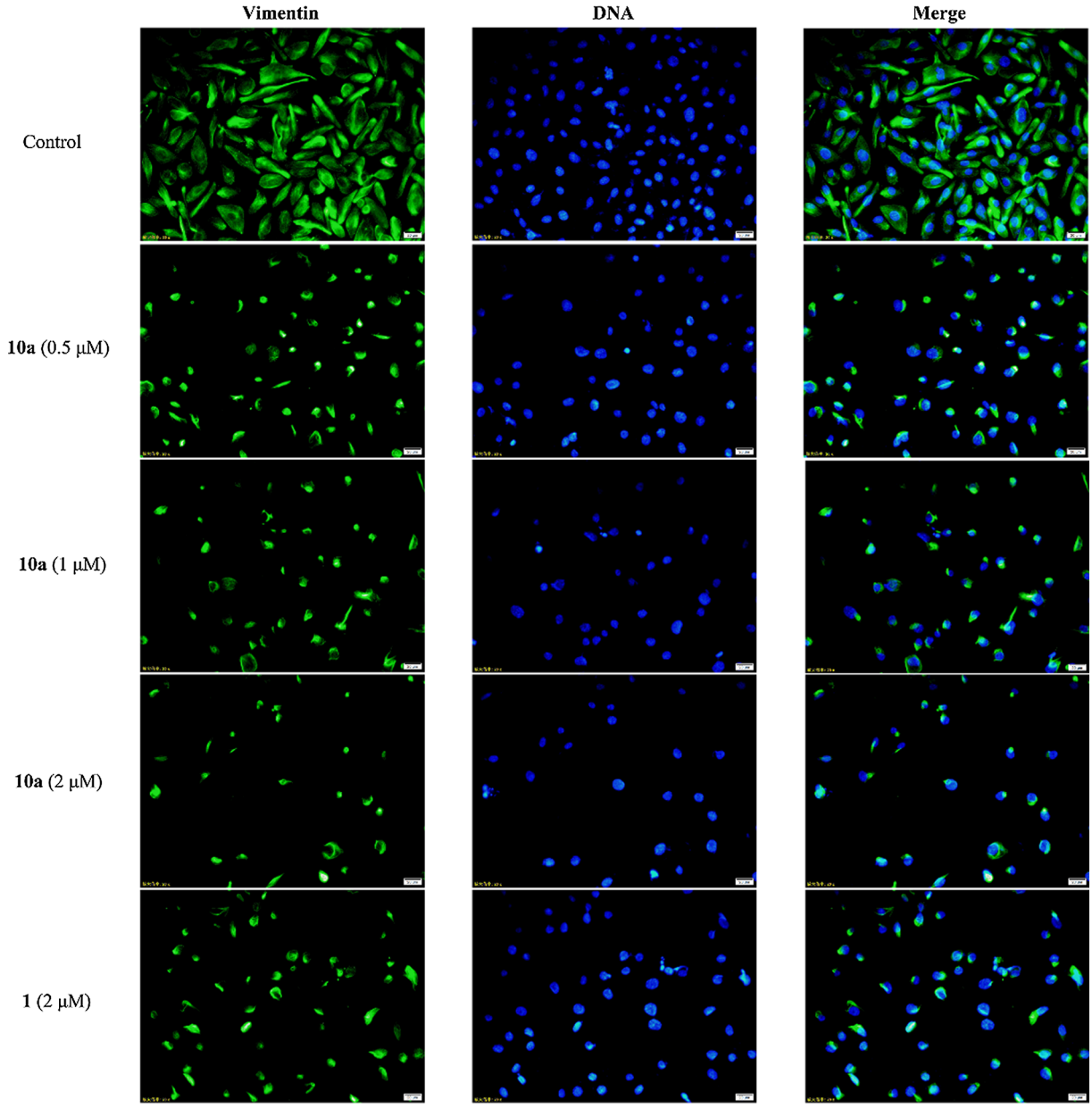

Fig. 11. Effects of **10a** on vimentin in A549 cells. A549 cells were incubated with vehicle, **10a** and **1** for 24 h, respectively. Vimentin and nuclei were stained with anti-vimentin antibody (green) and DAPI (blue), respectively. Magnification 20×.

126.00, 124.10, 114.72, 114.56, 113.93, 109.88, 108.37, 108.29, 105.46, 105.35, 101.44, 101.29, 100.65, 100.56, 72.62, 70.72, 67.89, 67.10, 60.83, 56.19, 55.32, 45.38, 44.15, 39.68, 33.79, 30.59, 28.35, 24.11, 21.41; HRMS-ESI (*m/z*): calcd for $C_{43}H_{41}O_{13}$ $[M+H]^+$ 765.2542, found 765.2531.

4.3. Pharmacology

4.3.1. 3-(4,5-Dimethylthiazol-2-yl)-2,5-diphenyltetrazolium bromide (MTT) assay

Cells were from the lab of Professor Zhiyong Qian (State Key Laboratory of Biotherapy/Collaborative Innovation Center of Biotherapy, West China Hospital, Sichuan University, China). Cells were seeded in 96-well plates and incubated for overnight at 37 °C in 5% CO_2 atmosphere. Then various amounts of compounds were added to the wells and then incubated further for 72 h. After treatment, the medium was removed, 20 μL of 5 mg L^{-1} MTT was added to each well, and then incubated at 37 °C for another 4 h. The resulting formazan precipitate was dissolved with 150 μL DMSO before measurement at 570 nm with an enzyme-linked immunosorbent assay reader. All these tests were repeated in triplicate.

For treatment with inhibitors, A549 cells were pretreated with inhibitor, Necrostatin-1 (10 μM) or Z-VAD-FMK (20 μM), for 1 h, and incubated with test compounds for 48 h. The cell survival rate was measured by above MTT assay.

4.3.2. AO/EB dual staining

A549 cells were seeded into 24-well plates and incubated for 24 h incubation. The cells were treated with the test compounds at 37 °C in 5% CO_2 for 24 h. The cells were stained with 20 μL of acridine orange/ethidium bromide dye for 5 min. Subsequently, the dye was washed with PBS, and the cells were observed and imaged under fluorescent microscope.

4.3.3. Wound healing assay

A549 cells were seeded on 6 well plates at 37 °C in 5% CO_2 for 24 h.

Subsequently, the cells were scratched by using a sterile pipette tip and washed twice with PBS to remove the floating cells, then incubated with test compounds or vehicle (DMSO) for 24 h. The images were photographed with an inverted microscope and further processed via Image-Pro Plus 6.0.

4.3.4. Transwell invasion assay

A549 cells were seeded onto the upper chamber wells with medium containing 0.5% FBS medium and incubated with different concentrations of compounds. The lower chambers were filled with 800 μL total medium (15% FBS) containing different concentrations of compounds as upper chambers. After 24 h incubation at 37 °C, non-invasive cells were scraped with a cotton swab, and the invaded cells were fixed with 4% paraformaldehyde for 10 min and stained with crystal violet for 15 min. Finally, images were taken with an inverted microscope, and further measured using Image-Pro Plus 6.0.

4.3.5. Immunofluorescence assay

A549 cells were grown in 24-well plates and treated with different concentrations of compounds. After 24 h treatment, cells were fixed with 4% paraformaldehyde for 20 min and further perforated with 0.5% Triton X-100 for 10 min. Then, cells were blocked by goat serum at room temperature for 30 min followed by incubation with α-tubulin/Vimentin/Caspase-8 primary antibody overnight at 4 °C. Next, cells were incubated with the corresponding Alexa Fluor 488 labeled goat anti-rabbit secondary antibody at room temperature for 1 h. Cell nuclei were stained by DAPI at room temperature for 15 min. Images were obtained under a fluorescence microscope.

4.3.6. Molecular modeling

Docking simulation was investigated using Schrödinger Maestro. The crystal structure of tubulin (PDB code 1SA0) was arranged using the protein preparation wizard. The synthesized compound (**10a**) used in the docking simulation was optimized using the LigPrep module, and further docked into colchicine binding site using Glide. The docking results were further analyzed using PyMOL.

4.3.7. Statistical analysis

Statistical significance was analyzed by Student's *t*-test. $P < 0.05$ was considered statistically significant.

Acknowledgments

This work was financially supported by the National Natural Science Foundation of China (81860622), China; Department of Science and Technology of Guizhou Province ([2017]1219), China; Joint Fund of the Department of Science and Technology of Zunyi City and Zunyi Medical University ([2018]27), China; National First-Rate Construction Discipline of Guizhou Province (Pharmacy) (YLXKJS-YX-04), China.

References

[1] W. Chen, R. Zheng, P.D. Baade, S. Zhang, H. Zeng, F. Bray, A. Jemal, X.Q. Yu, J. He, CA Cancer J. Clin. 66 (2016) 115.
[2] T. Rodrigues, D. Reker, P. Schneider, G. Schneider, Nat. Chem. 8 (2016) 531.
[3] M. Gordaliza, P.A. García, J.M.M. Del Corral, M.A. Castro, M.A. Gómez-Zurita, Toxicon 44 (2004) 441.
[4] R.A. Stanton, K.M. Gernert, J.H. Nettles, R. Aneja, Med. Res. Rev. 31 (2011) 443.
[5] Y.Q. Liu, J. Tian, K. Qian, X.B. Zhao, S.L. Morris-Natschke, L. Yang, X. Nan, X. Tian, K.H. Lee, Med. Res. Rev. 35 (2015) 1.
[6] A. Kamal, S.M. Ali Hussaini, A. Rahim, S. Riyaz, Expert Opin. Ther. Patents 25 (2015) 1025.
[7] C. Bailly, Chem. Rev. 112 (2012) 3611.
[8] M. Gordaliza, M.A. Castro, J.M.M. del Corral, A.S. Feliciano, Curr. Pharm. Des. 6 (2000) 1811.
[9] Z.Z. Wang, W.X. Sun, X. Wang, Y.H. Zhang, H.Y. Qiu, J.L. Qi, Y.J. Pang, G.H. Lu, X.M. Wang, F.G. Yu, Y.H. Yang, Chem. Biol. Drug Des. 90 (2017) 236.
[10] X. Zhang, K.P. Rakesh, C.S. Shantharam, H.M. Manukumar, A.M. Asiri, H.M. Marwani, H.L. Qin, Bioorg. Med. Chem. 26 (2018) 340.
[11] X.H. Xu, X.W. Guan, S.L. Feng, Y.Z. Ma, S.W. Chen, L. Hui, Bioorg. Med. Chem. Lett. 27 (2017) 2890.
[12] W.X. Sun, Y.J. Ji, Y. Wan, H.W. Han, H.Y. Lin, G.H. Lu, J.L. Qi, X.M. Wang, Y.H. Yang, Bioorg. Med. Chem. Lett. 27 (2017) 4066.
[13] L. Zhang, J. Wang, L. Liu, C. Zheng, Y. Wang, Y. Chen, G. Wei, RSC Adv. 7 (2017) 10601.
[14] A. El-Bakoush, O.A. Olajide, Int. Immunopharmacol. 61 (2018) 325.
[15] Z. Li, G. Zeng, X. Zheng, W. Wang, Y. Ling, H. Tang, J. Zhang, Biomed. Pharmacother. 106 (2018) 349.
[16] G. Qiu, W. Tian, M. Huan, J. Chen, H. Fu, Exp. Biol. Med. 242 (2017) 223.
[17] P. Mutai, E. Pavadai, I. Wiid, A. Ngwane, B. Baker, K. Chibale, Bioorg. Med. Chem. Lett. 25 (2015) 2510.
[18] X.Y. Wu, H. Xu, Z.F. Wu, C. Chen, J.Y. Liu, G.N. Wu, X.Q. Yao, F.K. Liu, G. Li, L. Shen, Oncotarget 6 (2015) 44563.
[19] A.L. Wang, Y. Li, Q. Zhao, L.Q. Fan, Mol. Med. Rep. 17 (2018) 7721.
[20] C. Kim, S.G. Lee, W.M. Yang, F. Arfuso, J.Y. Um, A.P. Kumar, J. Bian, G. Sethi, K.S. Ahn, Cancer lett. 431 (2018) 123.
[21] Y. Yang, Y. Zhao, X. Ai, B. Cheng, S. Lu, Int. J. Clin. Exp. Pathol. 7 (2014) 8453.
[22] J. Zhang, L. Liu, J. Wang, B. Ren, L. Zhang, W. Li, J. Ethnopharmacol. 221 (2018) 91.
[23] H.Y. Lin, W.X. Sun, C.S. Zheng, H.W. Han, X. Wang, Y.H. Zhang, H.Y. Qiu, C.Y. Tang, J.L. Qi, G.H. Lu, R.W. Yang, X.M. Wang, Y.H. Yang, RSC Adv. 7 (2017) 48404.
[24] Y. Li, F. Yang, L. Wang, Z. Cao, T. Han, Z. Duan, Z. Li, W.J. Zhao, Eur. J. Med. Chem. 112 (2016) 196.
[25] J. Ren, H.J. Xu, H. Cheng, W.Q. Xin, X. Chen, K. Hu, Eur. J. Med. Chem. 54 (2012) 175.
[26] D.J. Fu, L. Zhang, J. Song, R.W. Mao, R.H. Zhao, Y.C. Liu, Y.H. Hou, J.H. Li, J.J. Yang, C.Y. Jin, P. Li, X.L. Zi, H.M. Liu, S.Y. Zhang, Y.B. Zhang, Eur. J. Med. Chem. 127 (2017) 87.
[27] S. Mishra, P. Singh, Eur. J. Med. Chem. 124 (2016) 500.
[28] H.W. Han, H.Y. Qiu, C. Hu, W.X. Sun, R.W. Yang, J.L. Qi, X.M. Wang, G.H. Lu, Y.H. Yang, Bioorg. Med. Chem. Lett. 26 (2016) 3237.
[29] Y. Liu, D. Wei, Y. Zhao, W. Cheng, Y. Lu, Y. Ma, X. Li, C. Han, Y. Wei, H. Cao, C. Zhao, Bioorg. Med. Chem. 20 (2012) 6285.
[30] J. Wang, L. Long, Y. Chen, Y. Xu, L. Zhang, Bioorg. Med. Chem. Lett. 28 (2018) 1817.
[31] L. Zhang, J. Zheng, Y. Rong, C. Yang, L. Long, Y. Xu, Y. Chen, J. Wang, Q. Yao, Med. Chem. Res. 27 (2018) 2231.
[32] Y.D. Guo, Z.B. Wang, B.S. Wang, N. Li, Z.P. Zuo, China J. Tradit. Chin. Med. Pharm. 26 (2011) 560.
[33] H. Wu, X. Che, Q. Zheng, A. Wu, K. Pan, A. Shao, Q. Wu, J. Zhang, Y. Hong, Int. J. Biol. Sci. 10 (2014) 1072.
[34] P. Friedl, K. Wolf, Nat. Rev. Cancer 3 (2003) 362.
[35] S.S. Lin, K.C. Lai, S.C. Hsu, J.S. Yang, C.L. Kuo, J.P. Lin, Y.S. Ma, C.C. Wu, J.G. Chung, Cancer lett. 285 (2009) 127.
[36] M. Dauphin, C. Barbe, S. Lemaire, B. Nawrocki-Raby, E. Lagonotte, G. Delepine, P. Birembaut, C. Gilles, M. Polette, Lung Cancer 81 (2013) 117.
[37] L.S. Havel, E.R. Kline, A.M. Salgueiro, A.I. Marcus, Oncogene 34 (2015) 1979.
[38] A.M. Richardson, L. Havel, A.E. Koyen, J.M. Konen, J.A. Shupe, W.G. Wiles, W.D. Martin, H. Grossniklaus, G.L. Sica, M. Gilbert-Ross, A. Marcus, Clin. Cancer Res. 24 (2018) 420.
[39] R.B.G. Ravelli, B. Gigant, P.A. Curmi, I. Jourdain, S. Lachkar, A. Sobel, M. Knossow, Nature 428 (2004) 198.
[40] A. Giese, R. Bjerkvig, M.E. Berens, M. Westphal, J. Clin. Oncol. 21 (2003) 1624.